Karlsruher Institut für Technologie

Analytical and numerical solutions for swelling zones

Open Access am KIT

Theo Fett, Gabriele Rizzi

KIT SCIENTIFIC WORKING PAPERS 7

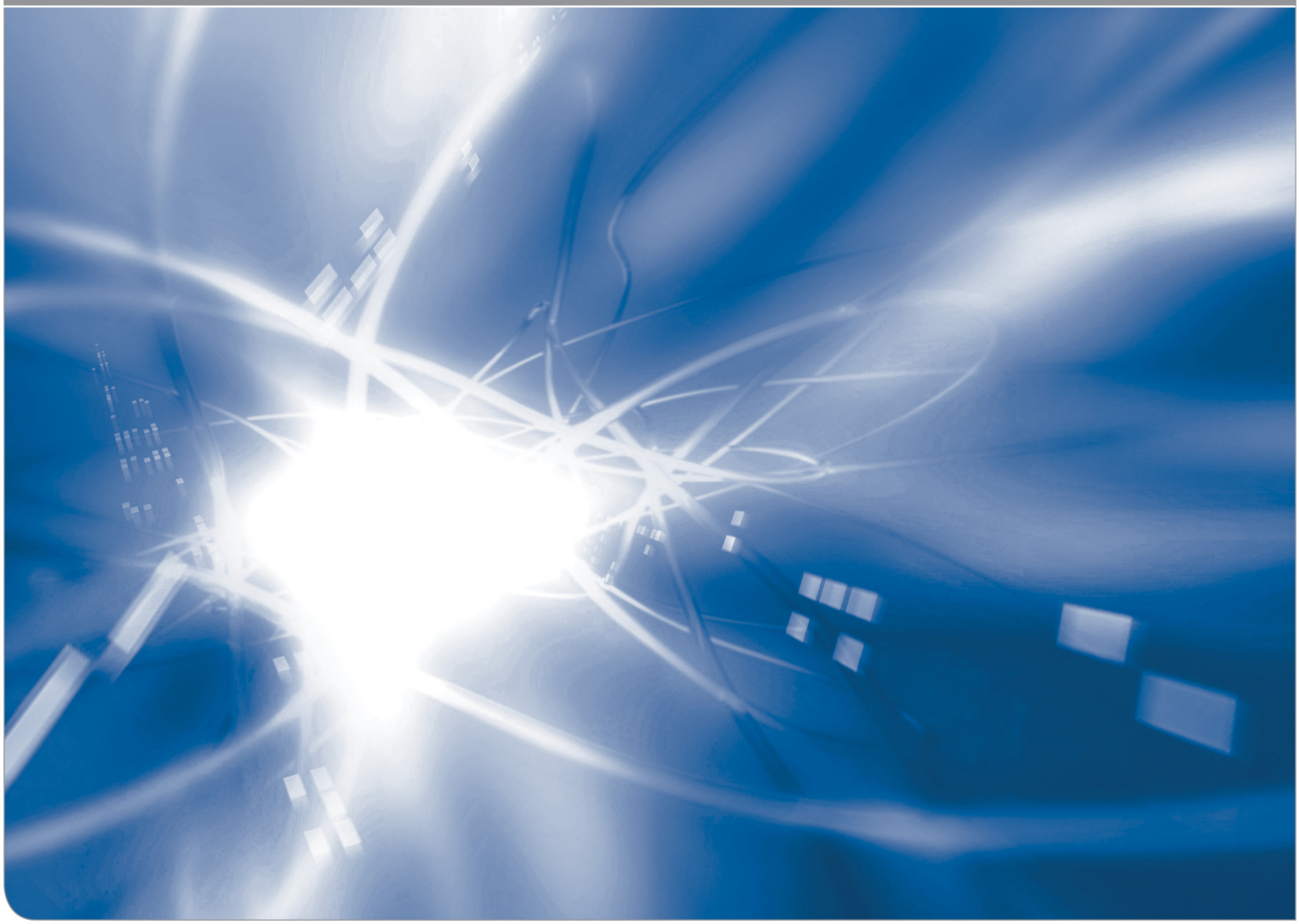

KIT – Universität des Landes Baden-Württemberg und nationales Forschungszentrum in der Helmholtz-Gemeinschaft

Institut für Angewandte Materialien, Karlsruher Institut für Technologie (KIT)

Impressum

Karlsruher Institut für Technologie (KIT)
www.kit.edu

2013

ISSN: 2194-1629

Abstract

Swelling of water-containing silica was reported very early in literature. As a consequence of the volume expansion in water diffusion zones swelling stresses must be generated which cause crack-tip shielding and crack opening effects.

In this short note, a number of fracture mechanics solutions is reported. The results are based on weight function computations and FE analyses. These solutions are not restricted to diffusion and swelling problems. They remain valid for any effect causing volume expansion as for instance ion-exchange zones in soda-lime glass.

Zusammenfassung

Schon in der frühen Glasliteratur wurde über das Schwellen von Quarzglas berichtet, das durch Wasseraufnahme verursacht wurde. Bei lokalem Einfluß von Wasserdiffusion in Glasoberflächen rißbehafteter Glasproben werden Druckspannungen in der Diffusionsschicht erzeugt, die zu Abschirmungs- und Rißöffnungseffekten führen.

In dieser Mitteilung wird über eine Reihe bruchmechanischer Lösungen berichtet, die durch Anwendung der Gewichtsfunktionsmethode und mit Finte-Element-Berechnungen erhalten wurden. Die Lösungen sind nicht speziell auf Wasserdiffusion beschränkt und können auch bei anderen Ursachen von Volumenexpansion (z.B. Ionenaustausch-Schichten in Natron-Kalk-Glas) verwendet werden.

Contents

1. Introduction

Water in silica reacts with the silica network according to

$$\equiv\text{Si-O-Si}\equiv + \text{H}_2\text{O} \leftrightarrow \equiv\text{SiOH}+\text{HOSi}\equiv \tag{1}$$

where the concentration of the immobile hydroxyl is [≡SiOH]=S and that of the mobile molecular water [H_2O]= C, [1]. This reaction is schematically illustrated in Fig. 1. The initial silica ring at which this reaction takes place will be broken with the consequence of a volume increase and a weakened mechanical cohesion.
Experimental evidence for swelling of water-containing silica was reported by Shelby [2]. As pointed out in [3], the volume swelling strain, ε_v, can be written

$$\varepsilon_v \cong 1.84 \frac{m_w}{m_w + m_{glass}} \tag{2}$$

where m_w is the amount of water per unit volume.

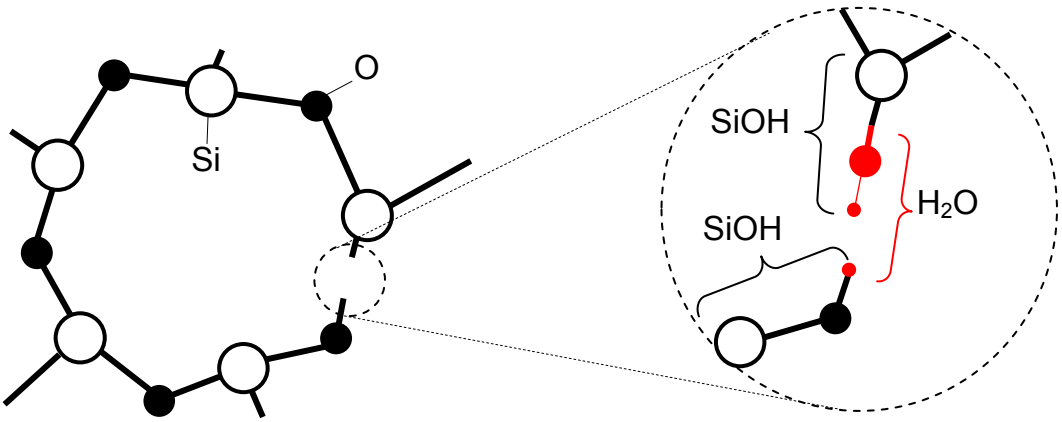

Fig. 1 Splitting of a glass ring by reaction with water.

2. Diffusion-controlled heart-shaped swelling zones

2.1 Stress-enhanced diffusion

The diffusion coefficient, D, which determines the rate of water diffusion into a solid depends on the stresses in the material and can be expressed by

$$D = D_0 \exp\left(\frac{\sigma_h \Delta V_w}{RT}\right) \tag{3}$$

where σ_h is the hydrostatic stress, Θ the absolute temperature, R the universal gas constant, and ΔV_w the activation volume for the diffusion of water in silica. Stress-

enhanced diffusion occurs especially in the singular stress field of mechanically loaded cracks where $\sigma \to \infty$.
If K denotes the stress intensity factor at the tip of a crack, then the singular near-tip hydrostatic stress field is given by the following equation:

$$\sigma_h = \tfrac{2}{3}(1+\nu)\frac{K}{\sqrt{2\pi r}}\cos(\varphi/2) \tag{4}$$

where r and φ are the the polar coordinates with origin at the crack tip. As outlined in [3], this results in heart-shaped diffusion and swelling zones around the crack tip, Fig. 2.

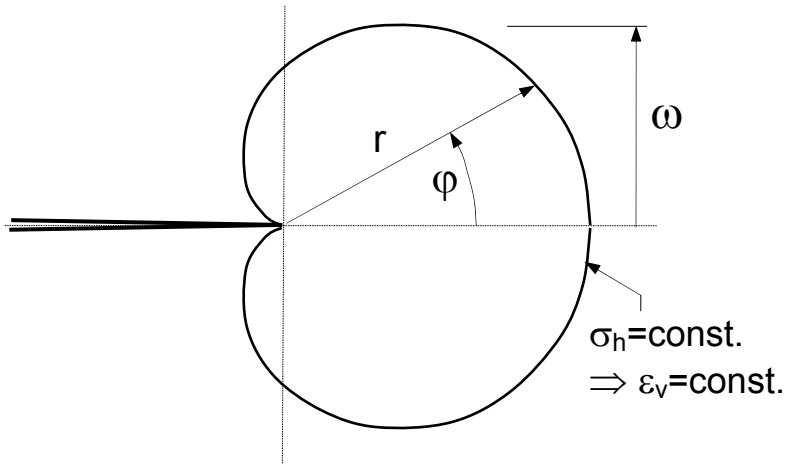

Fig. 2 Contour line for constant hydrostatic stress σ_h.

2.2 Shielding stress intensity factor

In order to compute the shielding stress intensity factor caused by an arbitrary radial distribution $\varepsilon_v(r)$, the case of a constant swelling strain may be used, Fig. 3a. For this zone, McMeeking and Evans [4] showed that

$$K_{sh} = 0 \tag{5}$$

Since this result does not depend on the zone height, ω, it results for variable swelling strains [5]

$$K_{sh} = \int_0^{\omega} \varepsilon_v \left(\frac{dK_{sh}(\omega')}{d\omega'} \right)_{\varepsilon=const} d\omega' = 0 \tag{6}$$

i.e. eq.(5) holds also in the case of any radial distribution of swelling, Fig. 3b.

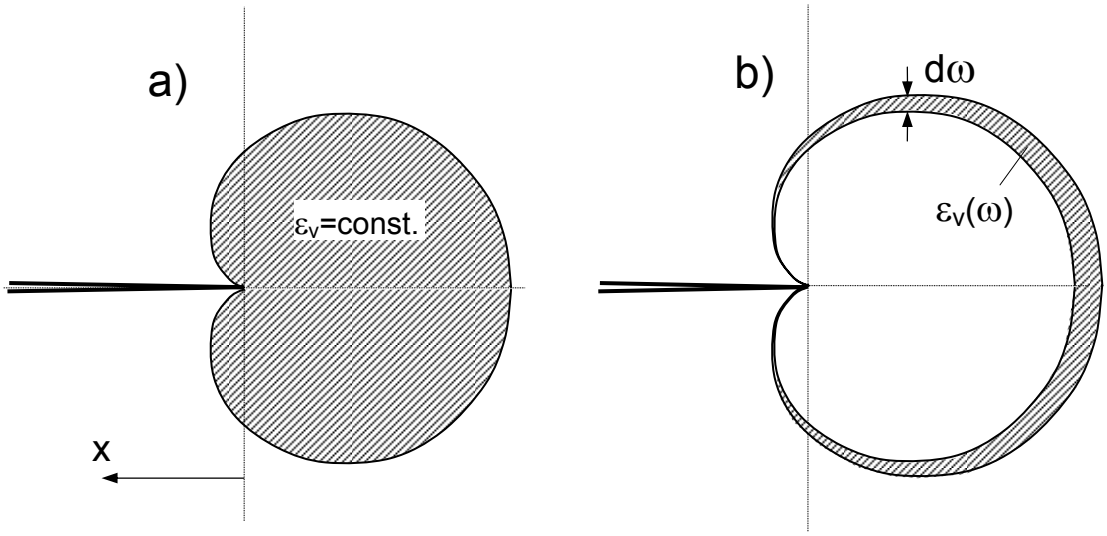

Fig. 3 a) Swelling zone with constant strain ε_v, b) zone increment with local strain $\varepsilon_v(\omega)$.

2.3 Crack opening displacement

Any stress intensity factor causes a square-root shaped near-tip crack opening displacement (COD) field as given by the Irwin equation

$$u_y = \sqrt{\frac{8}{\pi}} \frac{K}{E'} \sqrt{x} + O(x^{3/2}) \tag{7}$$

This must also hold for the shielding term $K_{\text{sh, eq.(3)}}$. Therefore, we have to expect disappearing COD for the heart-shaped swelling zone. Equation (7) does not imply that any crack opening displacement would disappear.

The displacements for a heart-shaped zone were computed in [6]. The results of this analysis, shown in Fig. 4, can be approximated by

$$u_y = \frac{p\,\omega}{E'} \frac{\tanh(1.395\,x/\omega)}{\sqrt[3]{1+10.64\,x/\omega}} \tag{8}$$

where p is that pressure that has to be applied on the heart-shaped zone contour to suppress any swelling strain [4]

$$p = \frac{\varepsilon_v E}{3(1-2\nu)} \tag{9}$$

The Young's modulus E' in eq.(8) stands for E in the case of plane stress and for $E/(1-\nu^2)$ for plane strain conditions (ν=Poisson's ratio).

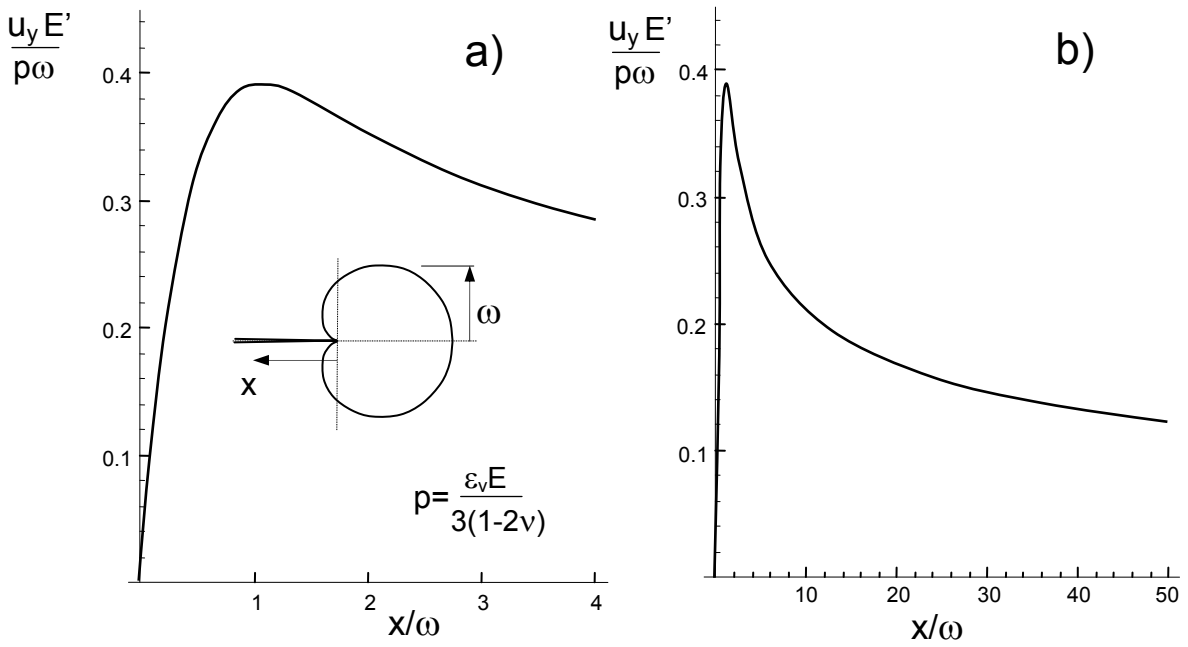

Fig. 4 Crack opening displacements in the crack wake for a heart-shaped swelling zone.

3. Elongated swelling zones

3.1 Swelling zones in thin sheets and plastic zones of the Dugdale type

From the images of crack tips in thin silica sheets reported by Bando et al. [7] a zone ahead of the tip can be detected that is very similar to those in mild steel as has very early be observed by Dugdale [8]. Figure 5 shows the crack opening displacement field for the water-soaked specimen. Whereas the solid profile is interpreted in [7] as that of the real crack, the dashed curve may be considered as a Dugdale zone of length $L \approx 55$nm.

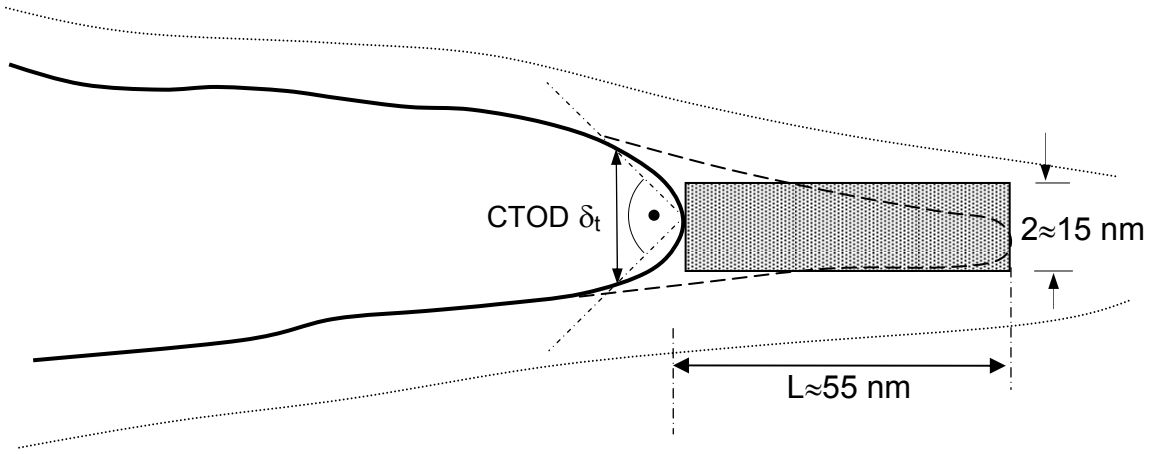

Fig. 5 Contours observed on Fig. 2B in [7]; Crack interpretation by Bando et al.

Because of this similarity, it seems not impossible that elongated zones ahead of crack tips may also occur in very thin silica sheets. Such zones will be modeled in the following considerations as narrow strips of length L and height H as shown in Figs. 5 and 6b, undergoing a constant volume expansion strain ε_v.

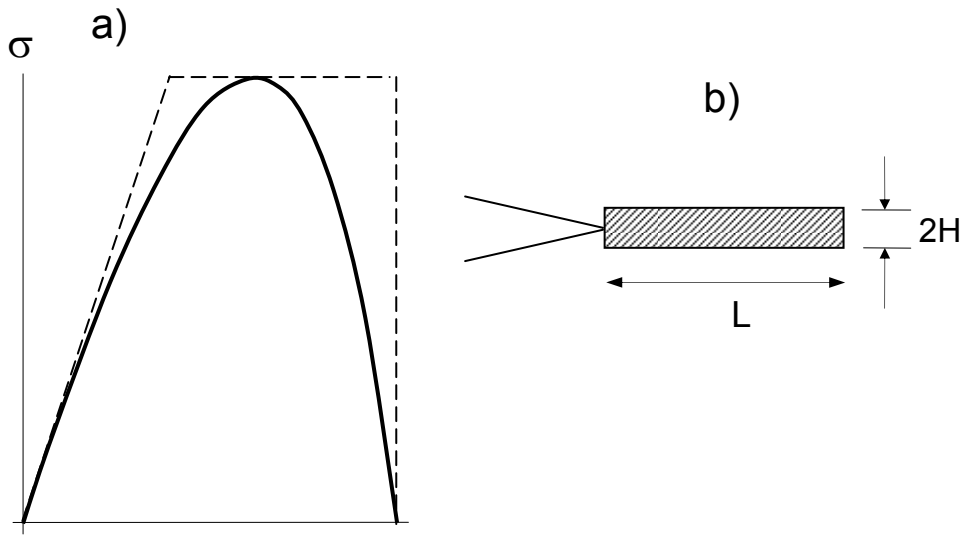

Fig. 6 a) Deformation behavior of elastic-ideal plastic materials (dashed) and silica (solid) including damage development by reaction between water and the glass structure [9], b) modeling of the strip-like swelling zones.

3.2 Computation of stress, stress intensity factor, and COD

3.2.1 Stress intensity factors

Stress intensity factors of swelling zones can be computed according to the suggestion by McMeeking and Evans [4] as the integral along the outer contour Γ of the swelling zone

$$K = p\int_{\Gamma} \mathbf{n}\cdot\mathbf{h}\, dS \tag{10}$$

where p is the stress necessary to restore the original size of the swollen zone, given in eq.(9), **h** is the vector of the weight function $\mathbf{h}=(h_x,h_y,0)^T$, and **n** is the vector normal to Γ. The near-tip weight function is given in [4].

Results for the stress intensity factor due to swelling are plotted in Fig. 7 for two cases. The results $K^{(1)}$ are for the real crack terminating at the left side of the swelling zone, the data $K^{(2)}$ belong to the fictitious crack as is used in the Dugdale model.
The results of Fig. 7 were fitted by the expressions

$$K^{(1)} = \frac{\varepsilon_v E}{1-\nu}\sqrt{H}\,0.34\tanh\left[\left(\frac{L}{H}\right)^{\lambda}\right]^{1/\lambda}, \quad \lambda=0.2928 \tag{11}$$

and

$$K^{(2)} = -\frac{\varepsilon_v E}{1-\nu}\sqrt{H}\,0.367\tanh\left[1.2945\left(\frac{L}{H}\right)^{1/2}\right] \tag{12}$$

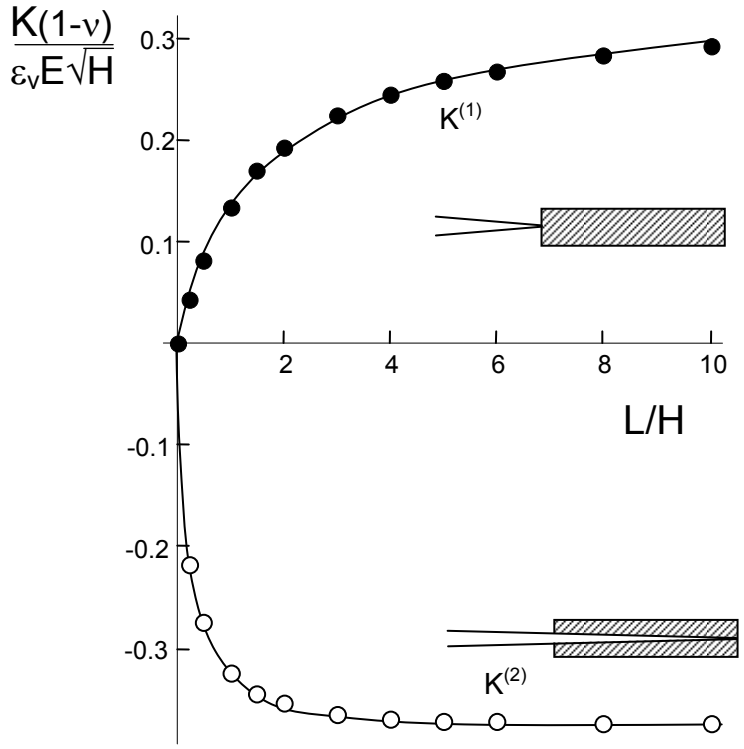

Fig. 7 Stress intensity factors for a crack terminating at the left side of a swelling zone (solid circles) and for the fictitious crack of the Dugdale model (open circles); curves were fitted to the data points.

3.2.2 Crack opening displacements

The crack surface displacements u_y (half of the total opening δ_{sw}) at the location ξ (Fig. 8a) are given by

$$u_y(\xi) = \frac{1}{E'}\int_{\xi}^{a}\frac{K_{sw}(a')}{\sqrt{a'-\xi}}da' \equiv \tfrac{1}{2}\delta_{sw} \tag{13}$$

where $K(a')$ is the stress intensity factor for a shorter virtual crack of length a' as illustrated in Fig. 8b. The stress intensity factor for the virtual crack $K(a')$ is again to be computed via eq.(10).

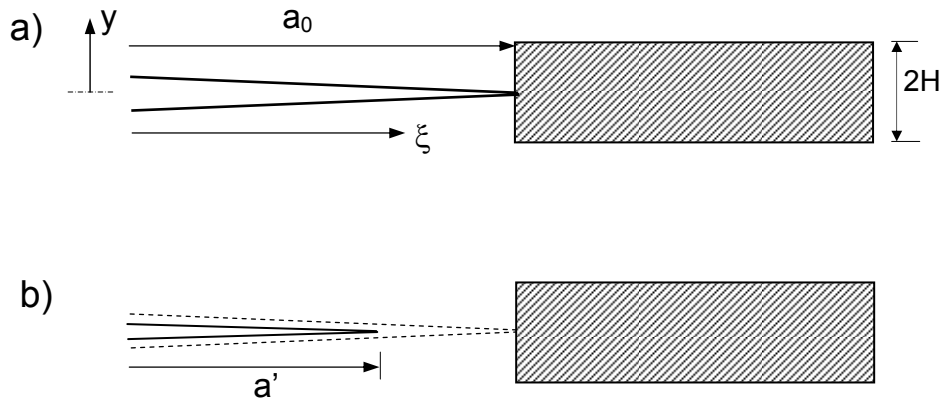

Fig. 8 a) Real crack of length a for which the displacements at location ξ should be computed, b) virtual crack of length $a'<a$ showing the stress intensity factor $K(a')$.

The stress intensity factors for virtual cracks of length a' are shown in Fig. 9a. Using these $K(a')$ data, eq.(13) was evaluated for a swelling zone with $L/H=4$. Figure 9b represents the total crack opening profile for a crack terminating at the beginning of the zone, the case of a real physical crack. This crack shows positive δ_{sw}, i.e. true opening exclusively caused by swelling. This result reflects the positive $K(a')$ on the left-hand side of Fig. 9a ($a'-a_0\leq 0$).

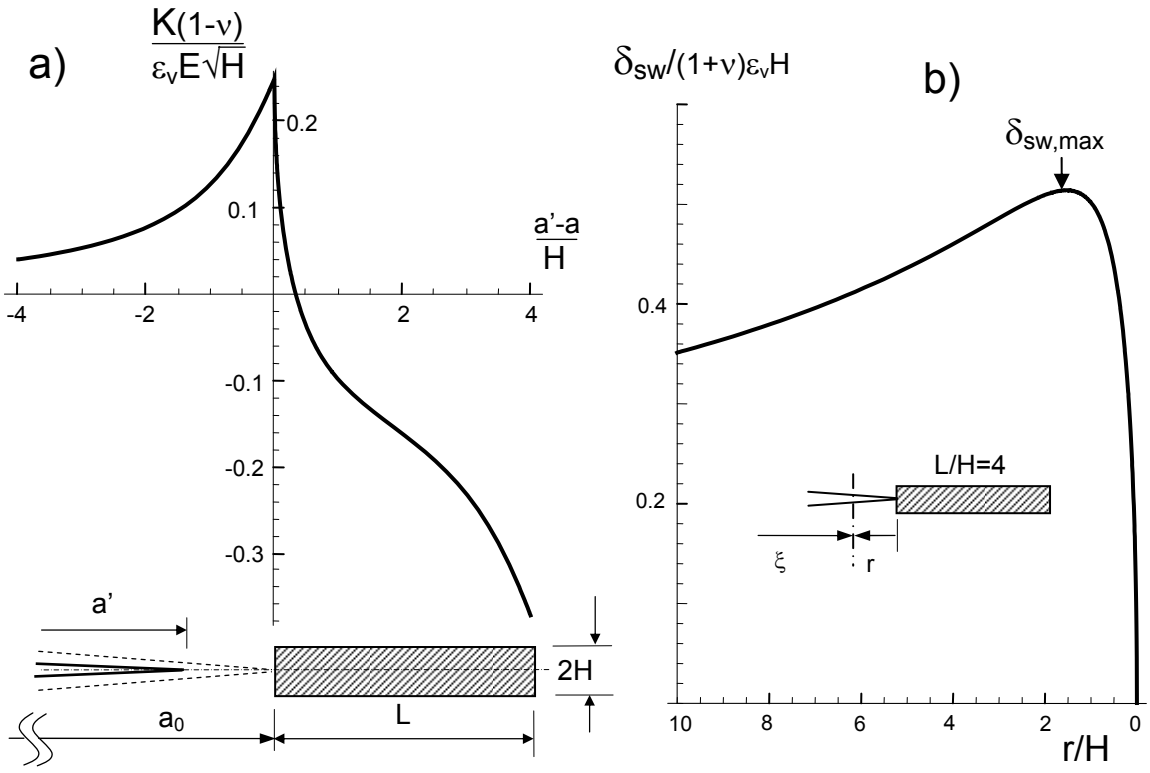

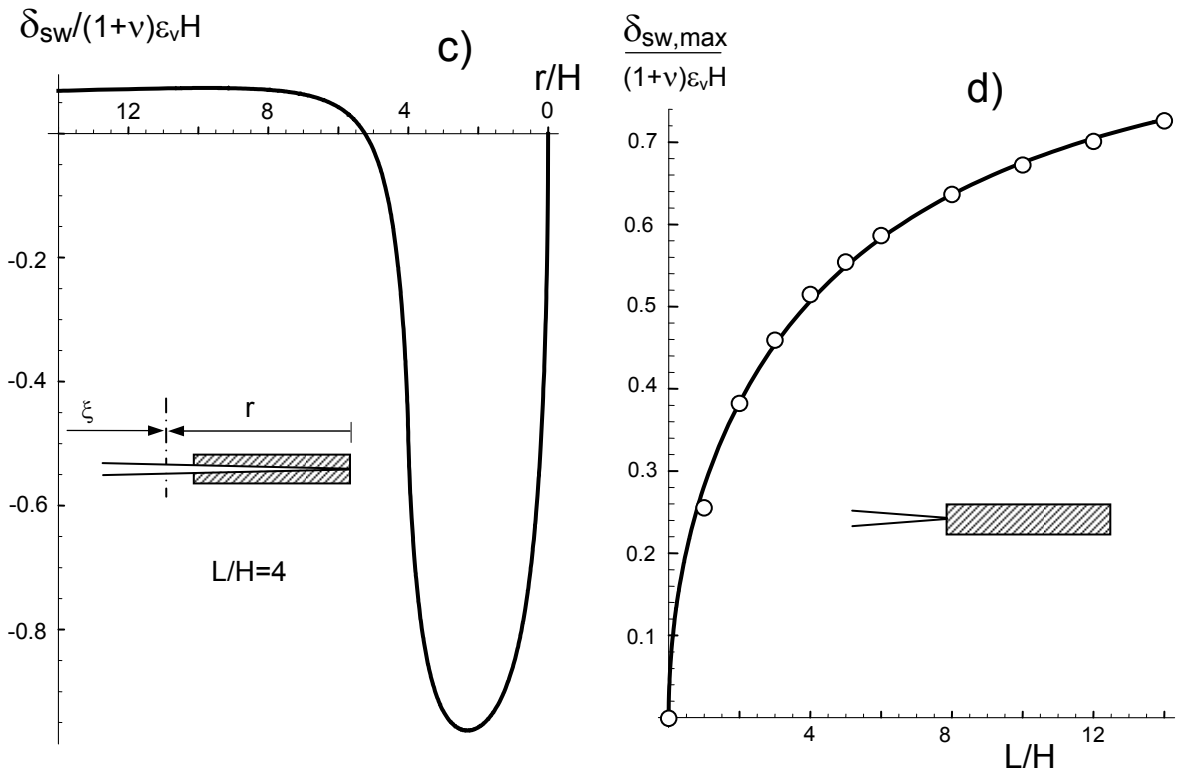

Fig. 9 a) Stress intensity factor $K(a')$ for virtual cracks (L/H=4, r=a-ξ), b) crack opening displacements by swelling, δ_{sw}, for a crack terminating at the beginning of the swelling zone, c) δ_{sw}, for a crack terminating at the end of the swelling zone, d) maximum swelling strain indicated by the arrow in Fig. 9b as a function of the ratio L/H.

In Fig. 9c, the COD-profile is shown for a crack terminating at the end of the zone (fictitious crack in the Dugdale model). This crack shows negative near-tip displacements, reflecting the negative stress intensity factors $K(a')$ on the right-hand side of Fig. 9a. Negative displacements with interpenetrating crack surfaces are of course not possible. This result tells us that the crack is closed in the absence of externally applied loading. The maximum opening displacement due to swelling is for the real crack plotted in Fig. 9d. The results can be approximated as

$$\delta_{sw,\max} \cong 0.846(1+\nu)\varepsilon_v H \tanh\left[0.3456\sqrt{\frac{L}{H}}\right] \qquad (14)$$

3.2.3 Computation of stresses

A weight function procedure for the determination of the stresses was developed in [10]. The stress at location ξ (Fig. 8a) is

$$\sigma(\xi) = \frac{1}{\sqrt{2\pi}} \frac{d}{d\xi} \left[\int_0^{\xi} \frac{K(a')}{\sqrt{\xi - a'}} da' \right] \tag{15}$$

By evaluation of this equation, the stresses for a swelling zone of L/H=4 were obtained as plotted in Fig. 10a. The average stress within the zone, defined as

$$\bar{\sigma} = \frac{1}{L} \int_0^L \sigma(r) dr \tag{16}$$

is plotted in Fig. 10b. An approximate description for L/H>>1 is given by

$$\bar{\sigma} \cong -0.367 \frac{\varepsilon_v E}{1-\nu} \left(\frac{H}{L} \right)^{0.725} \tag{17}$$

This approximation is introduced in Fig. 10b as the curve.

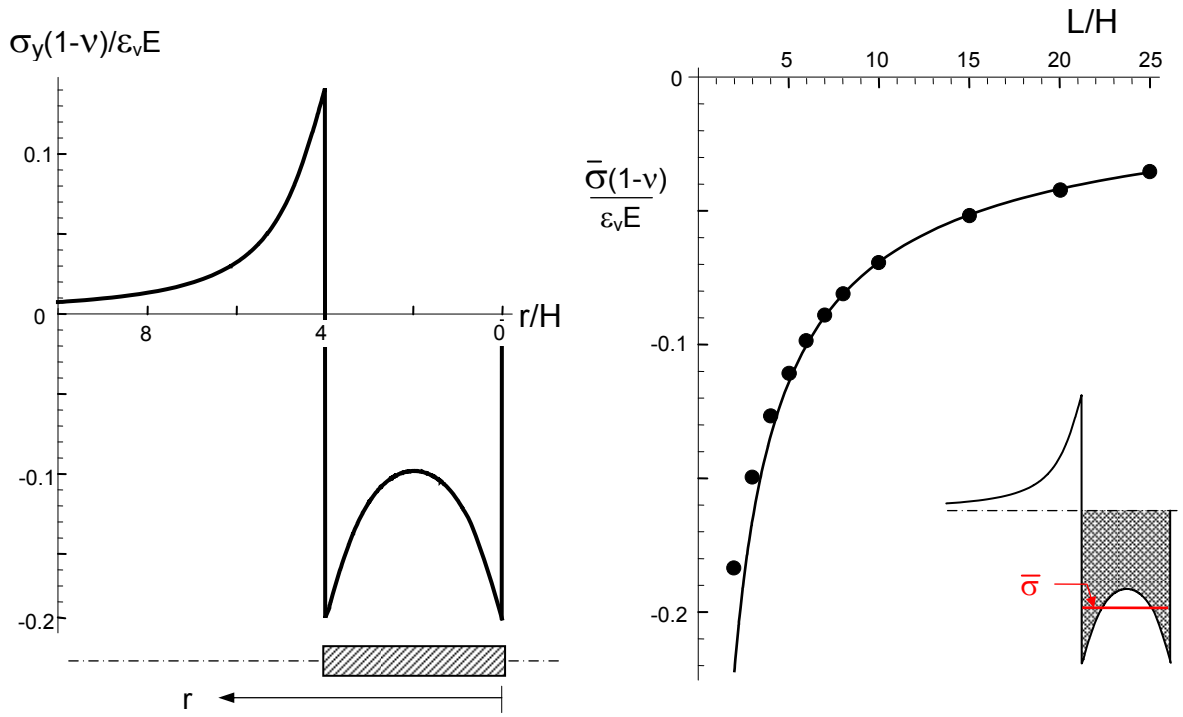

Fig. 10 a) Normal stresses σ_y along the symmetry line y=0 for a swelling zone of L/H=4, r=a-ξ, b) average stress in the swelling zone.

4. Some more results

4.1 Heart-shaped zone

4.1.1 Re-started crack

An arrested crack shows a heart shaped swelling zone at the tip. If the load is sufficiently increased, the crack will restart growing. We modelled by finite elements such a crack that passes the swelling zone of height ω. The case of the semi-infinite crack in an infinite body was realized by a plate of 60ω width and 30ω height including 1400 elements and 4300 node. Solid continuum elements (8-node biquadratic) in plane strain were chosen and the computations carried out with ABAQUS Version 6.8.

The results are shown in Fig. 11. Figure 11a represents the shielding stress intensity factor as a function of crack extension Δa after reloading as the squares. For Δa=0, the shielding term disappears as was analytically shown by McMeeking and Evans [11].

The T-stresses are given in Fig. 11b. This stress term represents the first regular stress term of the crack-tip stress field according to

$$\sigma_{ij} = \frac{K_I}{\sqrt{2\pi r}} f_{ij}(\varphi) + \sigma_{ij,0} \tag{18}$$

with

$$\sigma_{ij,0} = \begin{pmatrix} \sigma_{xx,0} & \sigma_{xy,0} \\ \sigma_{yx,0} & \sigma_{yy,0} \end{pmatrix} = \begin{pmatrix} T & 0 \\ 0 & 0 \end{pmatrix} \tag{19}$$

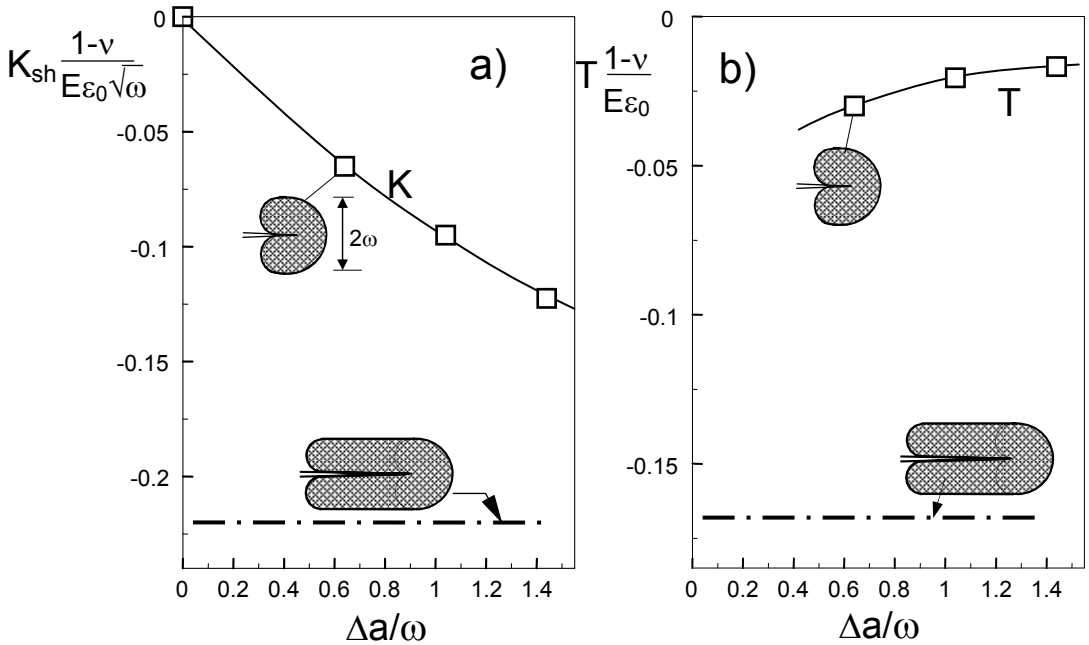

Fig. 11 FE-results for an arrested crack with heart-shaped swelling zone for additional crack extension Δa after reloading to a higher stress intensity factor, a) shielding stress intensity factor, b) T-stress term.

For Δa=0, the T-stresses taken along different mesh-contours did not converge. The dash-dotted lines in Fig. 6a and Fig. 6b indicate the values obtained for an extended zone with $\Delta a >> \omega$. From Fig. 6b, it becomes obvious that the T-term for the heart-shaped swelling zone is clearly smaller than in the case of an extended zone.

4.1.2 Displacements along the crack plane

When the crack has passed the swelling zone, the swelling strains can freely expand in *z*-direction. The displacements u_y resulting from FE computation are shown in Fig. 12. For the FE-analysis, a finite body had to be modeled. In the case of Fig. 12, a circular disc with a radius of 30ω was chosen. It has to be mentioned that the location of the base line for u_y is not free of problems and has to be matched to the practical problem that has to be solved. In a semi-infinite body the deformations normal to the free surface include a logarithm dependency of the form $\xi \times \log(\xi)$ that will have also far-distance influence (see e.g. Sections 30, 31 and 37 in [12]). We have to expect that a larger body will give larger displacements as can be seen from the finite slope in Fig. 12a at $\xi/\omega = \pm 30$.

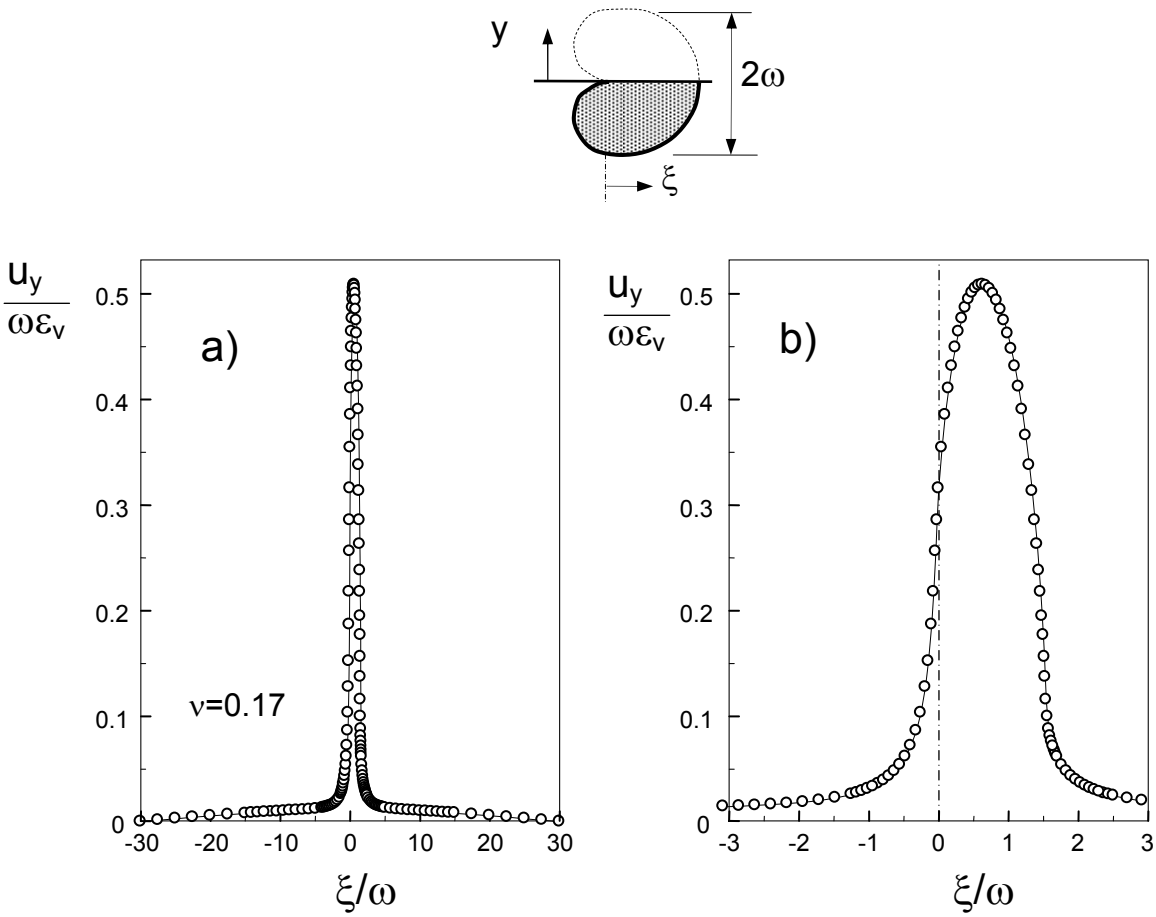

Fig. 12 Displacements in *z*-direction along the free surface for ν=0.17.

Since the Young's modulus in presence of water in hydroxyl form is reduced, we modelled the swelling zone with a smaller E_{sw} value of only 10% of the module for the surrounding material, E. The result plotted in Fig. 13 shows only a slightly reduced displacement of 10%.

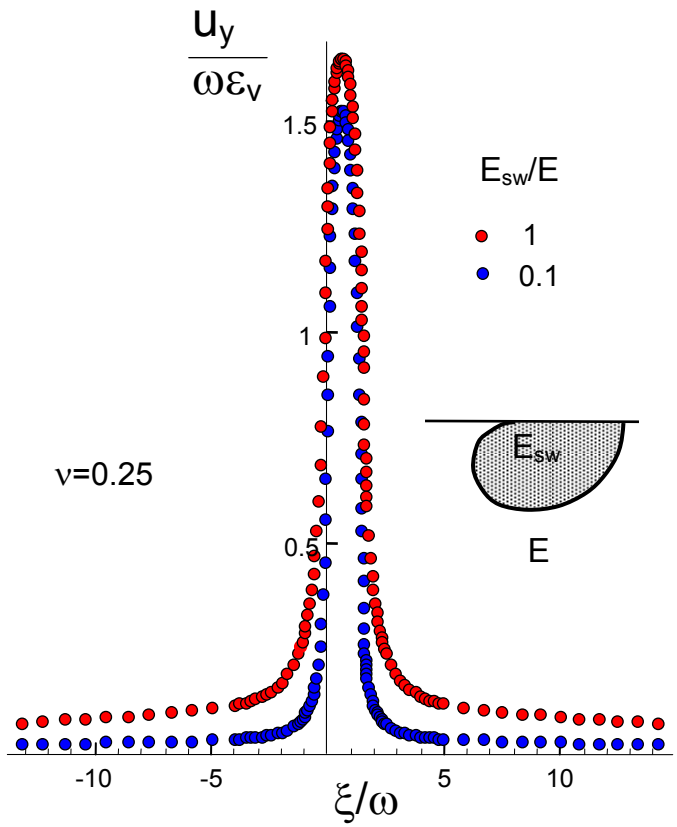

Fig. 13 Displacements for the ratio of Young's modulus ratios E_{sw}/E=1 and 0.1, ν=0.25.

4.2 Displacements of a swelling zone at its free end

A specimen that was soaked in water shows surface swelling zones (Fig. 14a). If this plate is fractured (Fig. 14b), the swelling stresses can relax near the newly built ends. This results in displacements δ_y normal to the new surface.

Finite element computations were performed. The diffusion or swelling zone was modelled by a zone of thickness b with a constant volume strain ε_y. The results are plotted in Fig. 15. The sign of the displacements is here negative because the lower surface was modelled with the expansion *against* the y-direction.

The result of Fig. 15b can be used for the determination of the diffusivity and the swelling strain. For this purpose, a bar is water soaked and then fractured. The two fracture surfaces are measured with AFM and compared with the FE result.

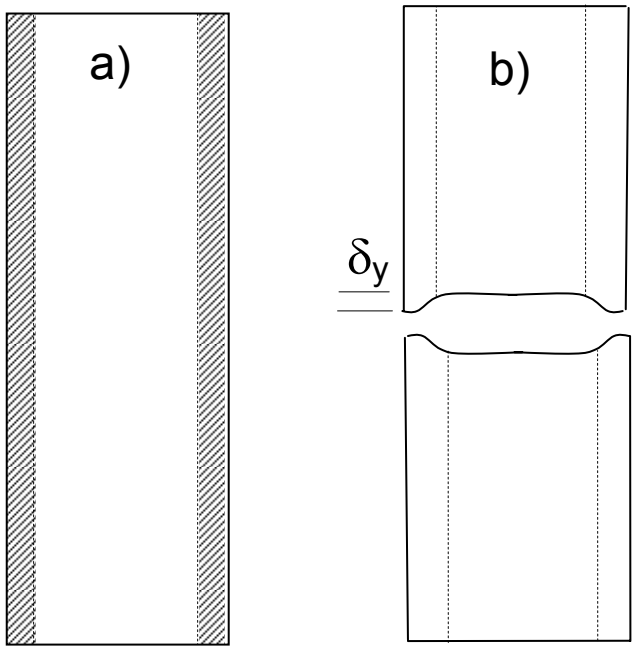

Fig. 14 a) Swelling zones on two sides of a plate, b) displacements on both sides of a specimen fractured after soaking.

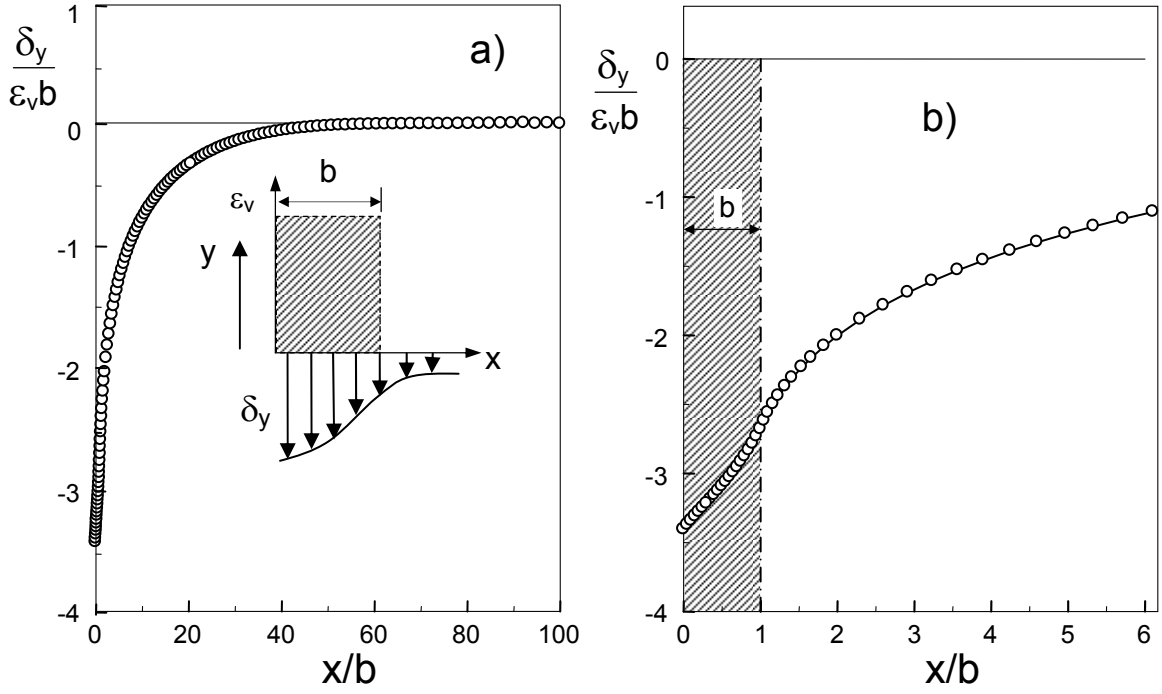

Fig. 15 Displacements at the end of a swelling zone.

References

1 Doremus, R.H., Diffusion of water in silica glass, J. Mater. Res. **10**(1995), 2379-89.

2. Shelby, J.E., "Density of vitreous silica," J. Non-Cryst. **349** (2004), 331-336.

3 S.M. Wiederhorn, T. Fett, G. Rizzi, S. Fünfschilling, M.J. Hoffmann and J.-P. Guin, "Effect of Water Penetration on the Strength and Toughness of Silica Glass," *J. Am. Ceram. Soc.* **94** [S1] S196-S203 (2011).

4 McMeeking, R.M., Evans, A.G., Mechanics of Transformation-Toughening in Brittle Materials, J. Am. Ceram. Soc. **65**(1982), 242-246.

5 S. M. Wiederhorn, T. Fett, G. Rizzi, M. J. Hoffmann, J.-P. Guin, The Effect of Water Penetration on Crack Growth in Silica Glass, Engng. Fract. Mech. **100**(2013), 3-16.

6 T. Fett, Application of the weight function and boundary collocation method to the calculation of initial phase transformation zones, Engng. Fract. Mech. **52**(1995), 853-863.

7 Y. Bando, S. Ito, M. Tomozawa, Direct Observation of Crack Tip Geometry of SO2 Glass by High-ResolutionElectron Microscopy, *J . Am. Ceram. Soc.,* 67 (1984), C36 C37.

8 D.S. Dugdale, "Yielding of Steel Sheets Containing Slits," *J. Mech. Phys. Solids*, **8**, 100-104 (1960).

9 T. Fett, S.M. Wiederhorn, Effect of water soaking in thin silica sheets on COD-behaviour, unpublished work.

10 T.Fett, E. Diegele, G. Rizzi, Calculation of stress fields near inclusions by use of the fracture mechanics weight function, Engng. Fract. Mech. **53**(1996), 17-22

11 McMeeking, R.M., Evans, A.G., Mechanics of Transformation-Toughening in Brittle Materials, J. Am. Ceram. Soc. **65**(1982), 242-246.

12 S.P. Timoshenko, J.N. Goodier, Theory of Elasticity,1973, McGraw-Hill Kogakusha, Ltd., Tokyo.

KIT Scientific Working Papers
ISSN 2194-1629

www.kit.edu